https://dx.doi.org/10.1016/j.bios.2022.114761



# Ultraminiature optical fiber-tip directly-printed plasmonic biosensors for label-free biodetection

Yangxi Zhang [a,†], Hao Wu [a,†], Han Wang [a], Bohan Yin [b], Siu Hong Dexter Wong [b], A. Ping Zhang [a,*], and Hwa-Yaw Tam [a]

[a] Photonics Research Institute, Department of Electrical Engineering, The Hong Kong Polytechnic University, Kowloon, Hong Kong SAR, China.

[b] Department of Biomedical Engineering, The Hong Kong Polytechnic University, Kowloon, Hong Kong SAR, China.

*** Corresponding author's email address**: azhang@polyu.edu.hk.

## Abstract

Miniaturization of biosensors has become an imperative demand because of its great potential in in vivo biomarker detection and disease diagnostics as well as the point-of-care testing for coping with public health crisis, such as the coronavirus disease 2019 pandemic. Here, we present an ultraminiature optical fiber-tip biosensor based on the plasmonic gold nanoparticles (AuNPs) directly printed upon the end face of a standard multimode optical fiber at visible light range. An in-situ precision photoreduction technology is developed to additively print the micropatterns of size-controlled AuNPs. The AuNPs reveal distinct localized surface plasmon resonance, whose peak wavelength provides an ideal spectral signal for label-free biodetection. The fabricated optical fiber-tip plasmonic biosensor can not only detect antibody, but also test SARS-CoV-2 mimetic DNA sequence at the concentration level of 0.8 pM. Such an ultraminiature fiber-tip plasmonic biosensor offers a cost-effective biodetection technology for a myriad of applications ranging from point-of-care testing to in vivo diagnosis of stubborn diseases.

**Keywords**: Gold nanoparticles, Additive printing, Plasmonic biosensor, Optical fiber sensors

## 1. Introduction

Highly sensitive and specific biodetection tools play a pivotal role in physiologic monitoring and disease diagnosis (Li et al., 2020). They are especially important in testing and monitoring of highly infectious diseases, for the purposes of preventing the transmission of diseases and providing timely treatment for patients (King et al., 2006; Wood et al., 2019). Particularly for the coronavirus disease 2019 (COVID-19), its long-incubation period and high percentage of asymptomatic cases have made the rapid and accurate diagnostic testing more important than ever (Vandenberg et al., 2021; Kevadiya et al., 2021). Although the reverse transcription polymerase chain reaction (RT-PCR) has currently become the gold standard of nucleic acid testing for COVID-19 (Surkova et al., 2020), it has the drawbacks of high consumption of reagents and relying on highly specialized operations. Therefore, it is urgently needed to

[†] Yangxi Zhang and Hao Wu contributed equally to the work.

develop miniaturized easy-to-use biodetection devices for point-of-care testing with minimal sample consumption.

Nanophotonic biosensors are one of the most promising candidates of high-sensitivity miniature biosensors because of their ability on harnessing the light to interact with matter at the micrometer and even nanometer scales for ultrasensitive biomolecular detection (Altug et al., 2022; Koenderink et al., 2015). In particularly, plasmonic sensors based on localized surface plasmon resonance (LSPR), i.e. optically excited collective oscillation of electrons, can be easily put into operation by using unpolarized light and simple optics-based spectral signal interrogation system (Mejía-Salazar et al., 2018; Zijlstra et al., 2012; Brolo et al., 2012; Talebian et al., 2020). The resonant wavelength of the LSPR nanostructures of many metals, such as Au, Ag, Al, and Cu, sensitively depends on the external refractive index of surrounding media via evanescent field, which thus have become a very promising candidate for high-sensitivity label-free biodetection. Especially, the gold nanoparticles (AuNP)-based LSPR biosensors attracted great attention in the development of cost-effective high-performance plasmonic biosensors due to their excellent chemical stability and good biocompatibility as well as the relative ease of preparation.

Like all other optical sensors, the main obstacle on achieving a miniaturized LSPR biosensor is optical excitation and coupling parts for acquiring intact spectral signal. Since optical fiber is a perfect waveguide that can deliver excitation light and collect optical signal with extremely low power loss, one of promising solutions to achieve miniaturized LSPR biosensors is to directly engineer optical fiber with plasmonic nanostructures to develop small-size optical fiber-based plasmonic biosensors (Kostovski et al., 2014; Consales et al., 2012; Xiong et al., 2020). A common approach to fabricate optical fiber-based plasmonic sensors is to micro-machine standard optical fibers so as to allow the light guided by the fiber core to wavelength selectively couple with the plasmons of metal nanofilm or nanostructures for LSPR biosensing. For example, optical fiber taper (Tuniz et al., 2018), D-shaped fiber(Cennamo et al., 2021) and fiber gratings(Caucheteur et al., 2016) were demonstrated by tapering/polishing optical fibers or UV exposure to make fiber-based plasmonic sensors. However, these micro-machine processes will either dramatically weaken the mechanical property of fiber sensors or increase fabrication cost. Alternatively, specialty optical fibers, such as hollow-core fiber (Ermatov et al., 2020) and U-bent fibers (Bandaru et al., 2020), were also demonstrated to develop optical fiber plasmonic biosensors. However, such specialty optical fibers are not only costly, but also not compatible with standard optical fibers, which thus hinder ease of use. Recently, optical fiber-tip devices with micro/nano-engineered fiber end-face attracted great interests because of their immense potential on the development of ultra-small ready-to-use photonic sensors and microsystems (Kostovski et al., 2014; Guggenheim et al., 2017). Nanofabrication technologies, such as two-photon polymerization (Kim et al., 2020), nanoimprint lithography (Kostovski,

et al., 2011), electron beam lithography (Sanders, et al., 2014), and focused ion beam (Principe, et al., 2017), were applied to fabricate ultrafine photoresist nanostructures and then transfer to plasmonic Au/Ag nanostructures for ultrasensitive Raman spectroscopy and label-free biosensing applications. However, these fabrication methods require the use of expensive facilities in a high-standard environment as well as extra deposition and etching/lift-off processes to convert the photoresist pattern to metal nano-structures due to their subtractive manufacturing nature. Such expensive and less convenient fabrication processes may nullify the advantages of LSPR biosensors for massive applications.

Here, we develop an ultraminiature optical fiber-tip plasmonic biosensor in which AuNPs are additively printed on the end face of a standard multimode optical fiber at visible range for label-free biodetection, as shown in Fig. 1. Our recently developed precision photoreduction technology (Zhang, et al., 2018, Zhang, et al., 2021) is further improved to enable direct printing of the micropatterns of size-controlled AuNPs on a micrometer-scale target position so as to cost-effectively fabricate ultra-small plasmonic biosensors. The additive printing nature of the method may solve the trade-off between high performance and low cost of LSPR biosensors for broad applications. Experiments are demonstrated that such an optical fiber-tip biosensor based on plasmonic AuNPs can be conveniently functionalized with biological molecule probes, such as antibodies and nucleic acid receptors, for high-performance label-free biodetection applications.

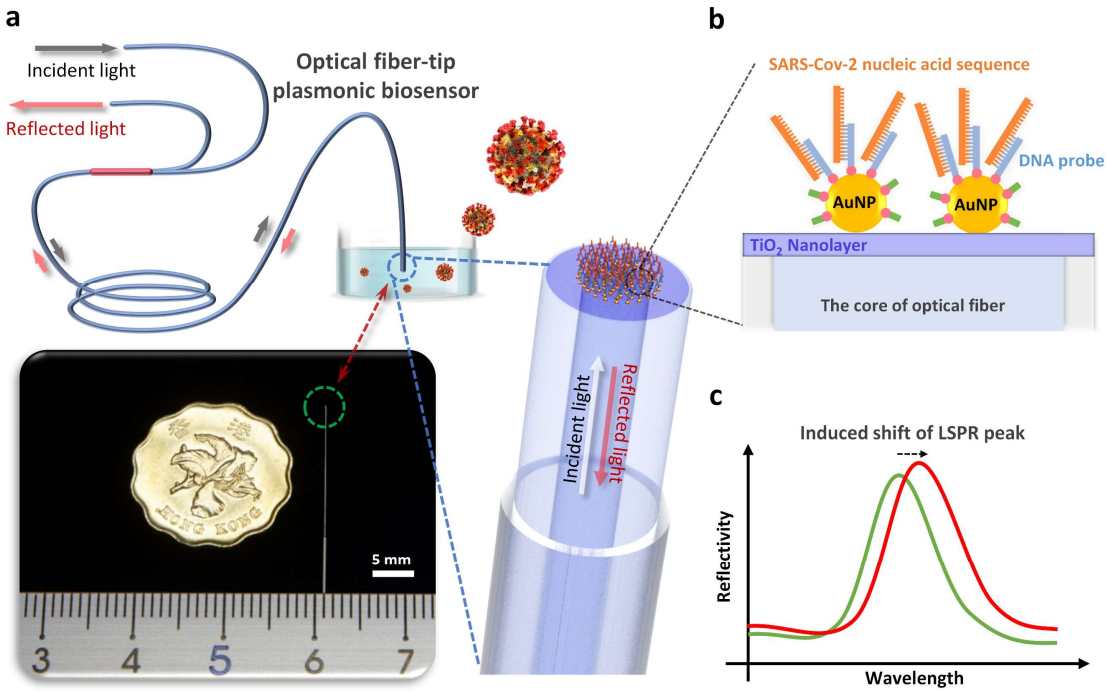


**Fig. 1.** Schematic and working principle of the printed optical fiber-tip plasmonic biosensor. (a) Schematic of the fiber-based plasmonic biosensor; (b) Schematic structure of the sensing part of the AuNPs-based plasmonic biosensor; (c) Working principle of the plasmonic biosensor.

## 2. Material and methods

### *2.1 Reagents and apparatus*

Gold(III) chloride hydrate, thiourea, potassium sodium tartrate tetrahydrate, citric acid trisodium salt dihydrate, titanium(IV) butoxide, cysteamine, glutaralldehyde, bovine serum albumin(BSA), sodium chloride, tris(2-carboxyethyl) phosphine(TCEP), 6-mecapto-1-hexanol(MCH), and phosphate buffered saline (PBS) were purchased from Sigma Aldrich Inc., USA. Nitric acid solution (1 mol $L^{-1}$) was purchased from Shenzhen Huashi Technology Co., Ltd., China. Isopropyl alcohol (IPA) was purchased from Anaqua Chemicals Supply Inc. Ltd., USA. Deionized (DI) water with a resistance of 18 mΩ·cm was used in all experiments.

Human IgG antibody was purchased from Sangon Biotech (Shanghai) Co., Ltd., China, and goat anti-Human IgG antibody was purchased from Beijing Solarbio Science & Technology Co., Ltd., China. SARS-CoV-2 N-protein-f receptor with 22 bases (CCCCTTGAAGAGGA-CGATCTTA) and SARS-CoV-2 Orf1-f receptor with 21 bases (GGGACAC-CCAAAATGTGAATT), which are modified by 5' Thiol C6 SS modifier amidite (6-((6-DMT-O-hexyl)-disulfonyl) hexan-1-ol) were purchased from Shanghai DNA Bioscience Co. Ltd., China. SARS-CoV-2 N-protein DNA sequence with 99 bases (Ggggaacttctcctgctagaatggctggcaatggcggtgatgctgctcttgctttgctgctgcttgacagattgaaccagcttgagagcaaaatgtctg), and SARS-CoV-2 orf-1 DNA sequence with 119 bases (Ccctgtgggttttacacttaaaaacacagtctgtaccgtctgcggtatgtggaaaggttatggctgtagttgtgatcaactccgcgaacccatgcttcagtcagctgatgcacaatcgt) were also purchased from Shanghai DNA Bioscience Co. Ltd., China. All materials were used as received without further purification.

The multimode visible-wavelength optical fiber (OM2 Multimode Fiber) was purchased from Yangtze Optical Fibre and Cable Joint Stock Ltd Co., China.

Optical microscopic images of the printed micropatterns of AuNPs on optical fiber-tip were taken by the optical microscope module of a laser scanning confocal microscope (VK-X200, Keyence Co. Ltd., Japan). Scanning-electron microscopy (SEM) images were taken by a field-emission scanning electron microscopy (MAIA3, Tescan, Czech). The optical spectra of the samples were measured by an optical spectrum analyzer (HR4000, Ocean Optics, USA), a broadband light source (ASBN-W050F, Spectral Products, USA) and a 3dB broadband fiber-coupler (TM50R582A, Thorlabs, USA).

### *2.2 Optical printing of fiber-tip plasmonic sensors*

An *in-situ* precision photoreduction technology is established to fabricate optical fiber-tip plasmonic biosensor by direct printing of size-controlled AuNPs on the end-surface of a standard multimode optical fiber (see Fig. S1 for more details). Firstly, the optical fiber was cleaved and mounted in a home-made spin-coating fixture. A thin layer of titanium dioxide ($TiO_2$) photocatalytic layer (< 20 nm) was uniformly coated on the fiber end-surface by a spin-coating technique. The $TiO_2$ precursor solution was prepared by added 1% (volume ratio) 1 mol $L^{-1}$ nitric acid aqueous solution into 2% titanium (IV) butoxide IPA solution. The acidified precursor solution was flited and used for spin-coating immediately (parameters: 500 rpm for 6 s and 3000 rpm/30 s; environment: 20 °C and 60 % RH). The optical fiber was baked at 110 °C in oven for 10 min. Notably, the deposition of $TiO_2$ nanolayer is a critical step and its precise control can significantly improve the repeatability of sensor fabrication.

Secondly, the optical fiber is cleaned with IPA and blown with nitrogen and then fixed to a home-made exposure fixture. A glass cuvette was made to contain the growth solution and provide a flat liquid surface. Then the growth solution was injection into the cuvette to immerse the optical fiber's end-face. The growth solution was mixed by 0.1 mol $L^{-1}$ gold (III) chloride hydrate solution, 0.4 mol $L^{-1}$ thiourea solution, 0.2 mol $L^{-1}$ potassium sodium tartrate tetrahydrate solution, DI water, and 0.2 mol $L^{-1}$ citric acid trisodium salt dihydrate solution at a volume ratio of 1:1:1:1:4, and was filtered before further use. Then the optical fiber was precisely aligned to a pre-set exposure position assisted by a digital camera-based machine vision technology.

UV light micro-patterns were then dynamically projected on the end face of optical fiber by our in-house digital-micromirror device (DMD)-based digital ultraviolet exposure system. The illumination intensity was about 1803 $mW \cdot cm^{-2}$. The exposure time is around 400 s. The optical resolution (i.e., the pixel size of light pattern) of the digital UV lithography setup is about 0.493 μm. With the UV exposure, AuNPs grew toward target size and forms a micropattern in the exposed area of optical fiber end-face (see Fig. S1). After exposure process, the optical fiber end-face was rinsed sequentially by using DI water and IPA and finally dried with a heat gun at 450 °C for 10 min to remove thiourea on the surface of AuNP and reshape AuNPs to more regular shape.

### *2.3 LSPR sensing principle*

The sensing principle of the optical fiber-tip plasmonic biosensor is based on the AuNPs induced spectrally selectively back-scattering of light at LSPR wavelength. The light scattering of gold spherical/ellipsoidal nanoparticles with a specific size (upon a dielectric substrate) can be modeled by Mie-Gans theory (Mie, 1908, Gans, 1912, Bobbert, et al., 1986, Ungureanu, et al., 2009), whose key mechanism can be described by using the scattering cross section ($C_{sca}$) as (Maier, 2007):

$$C_{\mathrm{sca}} = \frac{k^4}{6\pi}|r|^2 = \frac{8\pi}{3}k^4 r^6 \left|\frac{\varepsilon - \varepsilon_{\mathrm{m}}}{\varepsilon - 2\varepsilon_{\mathrm{m}}}\right|^2 \quad (1)$$

where $r$ is radius, $k$ is angular wavenumber ($2\pi/\lambda$). When the real part of the complex permittivity ε and the medium permittivity $\varepsilon_m$ satisfies the relationship $Re[\varepsilon(\lambda)] = -2\varepsilon_m$, the scattering cross section reaches the maximum value which leads to a spectral peak in the scattering spectrum (Xu-Peng, et al., 2019). The corresponding wavelength of LSPR scattering peak $\lambda_{max}$ can be expressed as (Chauhan, et al., 2021):

$$\lambda_{\max} = \lambda_{\mathrm{p}}\sqrt{2n_{\mathrm{m}}^2 + 1} \quad (2)$$

where $\lambda_p$ is the LSPR wavelength of AuNPs and nm is the refractive index (RI) of surrounding medium. The formula shows a near-linear relationship between RI and LSPR peak wavelength. To detect biomolecules, such as antibody or DNA, the surface of AuNPs is functionalized with bioreceptors that can selectively bind with target molecules. The binding between target biomolecules and bioreceptors on the surface of AuNPs will introduce a refractive index increment to surrounding medium near AuNPs (Tumolo, et al., 2004) and result in a shift of LSPR peak wavelength. If AuNPs are directly printed on the end face of an optical fiber, an ultraminiature plasmonic biosensor can be fabricated in which the LSPR signal can be highly efficiently collected by optical fiber for biodetection analysis.

### *2.4 Numerical simulation*

To numerically simulate the spectral responses of the optical fiber-tip plasmonic sensor, a commercial software (COMSOL Multiphysics) was used to model the AuNP-$TiO_2$-quartz structure on the end face of optical fiber. The AuNPs were modelled as periodic arrays in a square lattice. A linearly polarized light wave was assumed as the excitation light to illuminate the structure at the normal direction of incidence from the quartz side.

### *2.5 Functionalization for antibody detection*

To demonstrate the antibody detection ability, the optical fiber-tip plasmonic sensor was functionalized with a protein antigen (human IgG) to detect the target antibody (goat anti-human IgG). The fabricated fiber-tip plasmonic sensors were treated by cysteamine (5 mM, 20 °C, 1 h) and glutaraldehyde (1 wt%, 20 °C, 30 min) sequentially. Then human IgG antibody was immobilized upon cysteamine/glutaraldehyde coated AuNPs by immersion in $10^{-7}$ M human IgG/PBS solution (20 °C, 2 h). Bovine serum albumin (BSA) was used as blocking agent (1 wt% in PBS, 20 °C,1h). The biosensor after functionalization with antigen was stored in deionized water under 4 °C. In testing experiments, the sensor was immersed in goat anti-human IgG/PBS solution at 20 °C for 1 h.

### *2.6 Functionalization for nucleic acid detection*

The ability of the optical fiber-tip sensor for nucleic acid testing was experimentally tested by detection of SARS-CoV-2 mimetic DNA sequence, i.e. N-protein DNA sequence. The purchased SARS-CoV-2 thiolated single stranded DNA (SH-DNA) probes (i.e. SARS-CoV-2 N-protein-f receptor) was already modified with 5' Thiol C6 SS modifier. The SH-DNA probe was further treated with TCEP via a disulfide reduction process so as to enable strong bonding to AuNPs with Au-S bond. 1 μM SH-DNA probe was treated with 200 μM TCEP at 20 °C for 1 h. The optical fiber-tip plasmonic sensor was then immersed in 2 mL N-protein-f receptor solution at 20 °C for 5 h. 0.2 mL 2 M NaCl solution was repeatedly added with the time interval of 30 min for total 10 times. Then, 5 mM MCH solution was used to block the unbinding region on AuNP at 20 °C for 1 h. The biosensor after functionalization was stored in deionized water at 4 °C. Target DNA sequence (i.e. N-protein DNA sequence) was diluted in deionized water. In testing experiments, the sensor was immersed in target DNA solution at 37 °C for 1 h.

## 3. Results

### *3.1 Printed micropatterns of gold nanoparticles*

Fig. 2a shows the optical microscopic images of the printed micropatterns of AuNPs on the end face of optical fiber, whose size is as small as 125 μm in diameter. It can be seen that various micro-patterns with arbitrary shapes are precisely printed around the center of optical fiber end-face. More microscopic and SEM images of the fabricated samples are given in Fig. S2, which reveal the flexible micro-printing ability of the *in-situ* precision photoreduction technology, particularly its direct printing ability on a very small target position like the end face of optical fibers. The material attribute of printed AuNPs was verified by an X-ray diffraction (XRD) analysis. As shown in Fig. S3(a), the XRD result shows clearly the typical peaks of Au crystal. To show the stability of printed AuNPs, a heat aging test at 450 °C was carried out, as shown in Fig. S3(b). The reflection spectral peak of the sensor has a small change after long-time high-temperature heating, which reveals the good stability of AuNPs printed in experiments.

One of the unique features of such a printing technology is the light-controlled growth of AuNPs towards target size by precise and quantitative regulation of UV exposure doses. Fig. 2a(iv) shows the circular patterns of AuNPs printed with different exposure doses. Their images at nanometer scale are shown in Fig. 2b, and their corresponding particle size distributions are given in Fig. S4. To make AuNPs with smooth surface, a thermal treatment (at 450 °C for 10 minutes) is applied to reshape the printed AuNPs, as shown in Fig. S5. It can be seen that the size of AuNPs proportionally increases with exposure

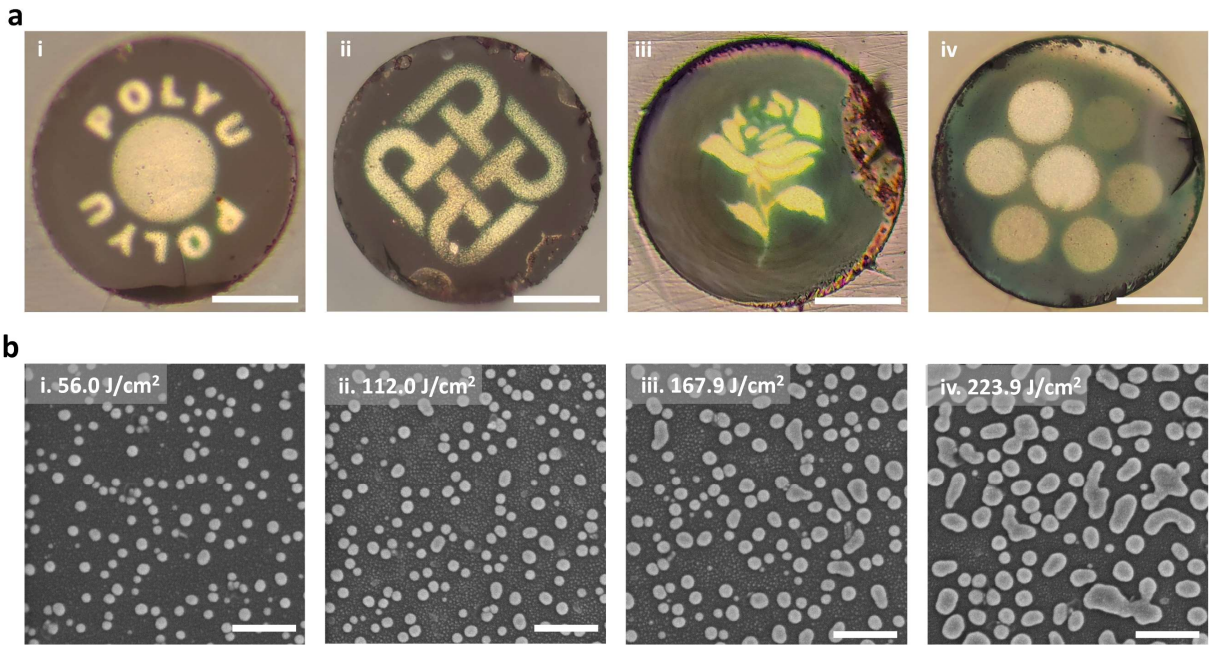


**Fig. 2.** Microscopic and SEM images of the printed AuNPs. (a) Optical microscopic images of the printed micropatterns of AuNPs on optical fiber end-face. i & ii. University name and logo; iii. Flower; iv. Circles with AuNPs of different sizes. The scale bars are 40 μm. (b) SEM images of the AuNPs of different size printed with different UV exposure doses. The scale bars are 400 nm.

doses. When their sizes are small, the shape of the printed AuNPs are relatively circular. With the increase of exposure doses, some noncircular large nanoparticles appear, which mainly result from the connection between adjacent AuNPs in thermal reshaping. Fortunately, LSPR biosensing needs not very large AuNPs, but these with the medium size of 70 ~ 100 nm in diameter, which renders the printing technology very effective in rapid fabrication of such optical fiber-tip AuNPs-based plasmonic biosensors.

### *3.2 Spectral characterization of printed plasmonic biosensors*

The reflection spectra of the optical fiber-tip LSPR biosensor were measured and compared with numerical simulation results. Fig. 3a(i) and (ii) show the measured reflection spectra of two sensors with the AuNPs of different dimension. When the size of AuNPs is around 70 nm, the reflection spectrum shows a spectral dip together with a small hump. When the particle diameter increases to 100 nm, a clear LSPR peak appears around 520 nm. If immerse the two sensors into a liquid with the refractive index higher than 1.333, the reflection spectra of both sensors show a stronger reflection peak. Both reflection peaks become stronger and shift to the longer wavelength with the increase of the refractive index of surrounding medium (from 1.333 to 1.431). The dependences of their LSPR peaks on the change of surrounding RI are summarized in Fig. 3a (iii). It can be seen that sensor 2 with larger AuNPs has a higher

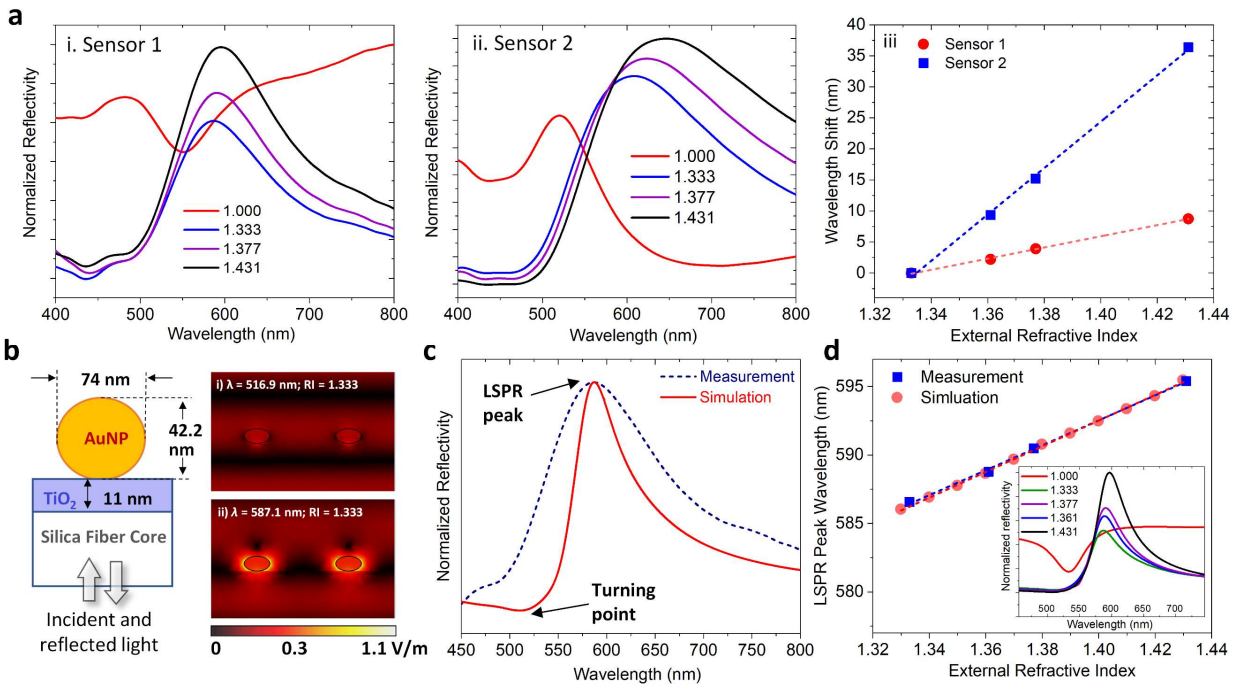


**Fig. 3.** Measurement and simulation of the spectral responses of optical fiber-tip plasmonic sensors. (a) Measured reflection spectra of the sensors: i. Sensor 1 based on 70-nm AuNPs; ii. Sensor 2 based on 100-nm AuNPs; iii. Spectral responses of the two sensors to the change of external refractive index. (b)Simulation model and the calculated electric field distribution at the turning point or LSPR peak wavelengths. (c) Comparison between the measured and simulated spectra of sensor 1 when the external refractive index is 1.333; (d) Comparison between the measured and simulated spectral responses of sensor 1 to the change of external RI. The simulated reflection spectra are given in the inset.

sensitivity (371.0 nm/RIU vs 89.2 nm/RIU). However, the reflection peak of sensor 2 is broader and thus its spectral resolution is relatively lower.

To understand the spectral responses of the fabricated optical fiber-tip AuNPs-based plasmonic sensors, numerical model is established according to the geometric information of AuNPs obtained by SEM, as also shown in Fig. 3. Fig. 3b shows the reflection spectra of the model when the size of the AuNPs is ~74 nm. Since the detection of biomolecules is performed in aqueous solution, the reflection spectra of sensor 1 in the medium with the RIs of 1.333 and 1.431 are simulated and shown in Fig. 3c and Fig. 3d. It can be seen that the peak wavelengths of the simulated results match very well with the measured spectra. The linewidths of the simulated peaks are narrower than the measured results, which mainly result from the size variance of the fabricated AuNPs.

The effect of the titanium dioxide nanolayer on the spectral response of the optical fiber-tip plasmonic sensor is also evaluated by numerical simulation. It revealed that the Fabry-Perot cavity effect formed by $TiO_2$ layer is relatively significant when the size of AuNPs is small and/or the sample is in air. However, the effect is partially suppressed when the sample is put into a liquid because the reflection of light from $TiO_2$/liquid interface is much weaker than that from $TiO_2$/air counterpart. An ultra-thin $TiO_2$ nanolayer

can also suppress such an interference effect and thereby a very thin TiO2 nanolayer (thickness < 20 nm) was used in the sensor fabrication.

### *3.3 Antibody detection*

Antibody testing has excellent specificity and can accurately identify disease-infected individuals, and therefore is widely used in seroepidemiologic and protective immunity studies for vaccine development (Iyer, et al., 2020). The optical fiber-tip plasmonic sensor was used in detection of goat anti-human IgG to verify the antibody detection ability. Fig. 4a shows the modification and detection processes for of antibody detection, with the modification of human IgG, the LSPR peak of the biosensor shifted to longer wavelength, see Fig. 4b. The results of the detection on target antibody, i.e. goat anti-human IgG, in solution by use of the antigen-functionalized optical fiber-tip plasmonic biosensor at the room temperature, are given in Fig. 4c. It can be seen that the sensor can be used to detect target antibody at different concentrations ranging from 100 ng/mL to 50 μg/mL. The limit of detection (LOD) was calculated by the triple of standard deviation to be <100 ng/mL, and the sensitivity is ~0.062 nm/nM in the range of 1 μg/mL ~ 10 μg/mL (i.e. 6.7 nM ~ 67 nM). Fig. 4d shows the measured response curves of

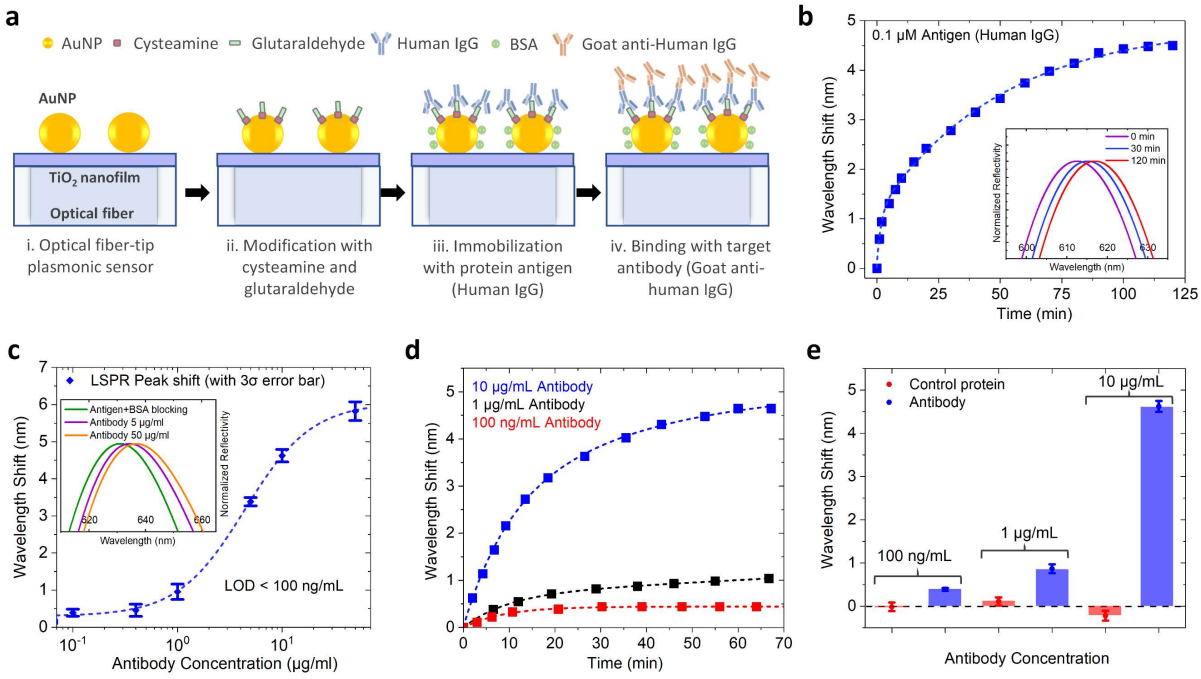


**Fig. 4.** Detection of goat anti-human immunoglobulin G (IgG). (a) Schematics of surface functionalization and antibody detection principle. (b) Wavelength shift of the biosensor's LSPR peak of the biosensor during the functionalization with antigen, i.e. human IgG. (c) Responses of the biosensor to different concentrations of target antibody, i.e. goat anti-human IgG. (d) Dynamic response of the biosensor to the target antibody solutions of different concentrations. (e) Specificity testing result by comparing the responses to the antibody and control protein BSA.

the biosensor, from which it can be seen that 90%-response times of the sensor to 100 ng/mL, 1 μg/mL, and 10 μg/mL target antibody solutions are 20.5 min, 36.8 min, and 38.8 min, respectively. The specificity of the biosensor was also tested by comparing the responses of the sensor to the target antibody and control protein BSA. As shown in Fig. 4e, the responses of the sensor to the BSA solutions at the concentrations of 100 ng/mL, 1 μg/mL, and 10 μg/mL are 0.03, 0.12, 0.047 times of the responses to goat anti-human IgG, which indicate a very good specificity of the sensor.

### *3.4 Nucleic acid detection*

Since the nucleocapsid protein (N-protein) and open reading frame 1ab (Orf1) gene are well known feature sequences of SARS-CoV-2 RNA (Sheikhzadeh, et al., 2020), the ability of the optical fiber-tip sensor in nucleic acid testing was experimentally tested by detection of SARS-CoV-2 mimetic DNA sequence, i.e. N-protein DNA sequence. As shown in Fig. 5a, a SH-DNA probe, i.e. SARS-CoV-2 N-protein-f receptor modified with 5' Thiol C6 SS modifier, is adopted to functionalize the optical fiber-tip sensor. With the modification of DNA probe, the LSPR peak of the biosensor shifted to longer wavelength, see Fig. 5b. The optical fiber-tip plasmonic biosensor can detect viral mimetic DNA sequence via

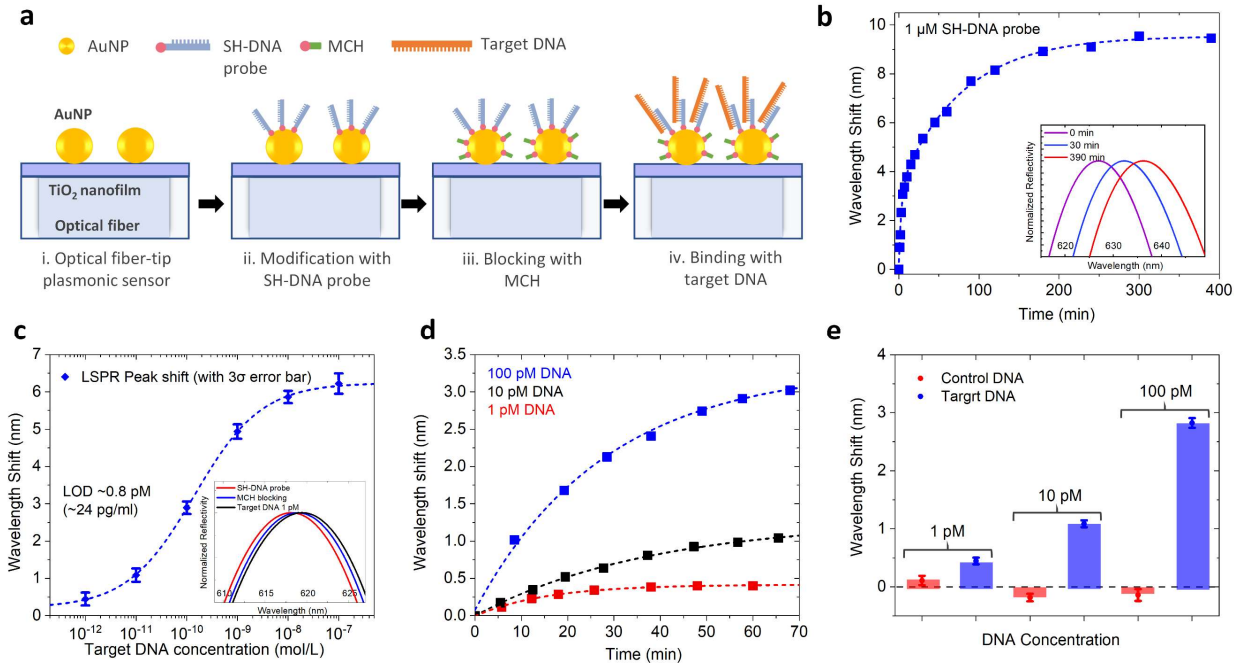


**Fig. 5.** Detection of SARS-CoV-2 mimetic DNA sequence. (a) Schematic of the surface functionalization and the nucleic acid testing principle. (b) Wavelength shift of the biosensor's LSPR peak during surface functionalization. (c) Responses of the biosensor to different concentrations of target DNA, i.e. N-protein DNA sequence. (d) Response curves of the biosensor to the target DNA solutions of different concentrations. (e) Specificity testing result of the sensor functionalized with N-protein-f receptor. Target DNA and control DNA are N-protein DNA sequence and Orf1 DNA sequence, respectively.

hybridization of SH-DNA probe and target DNA sequence. The measured result for detection of N-protein DNA sequence at the concentrations ranging from 1 pM to 100 nM are given in Fig. 5c. The LOD of the biosensor is estimated by using the triple of standard deviation to be ~0.8 pM (i.e. ~24 pg/mL). The sensitivity is ~0.024 nm/pM in the range from 1 pM to 100 pM. Fig. 5d is the measured response curves of the biosensor in the measurement of target DNA at the concentrations of 1 pM, 10 pM and 100 pM, from which one can see that the 90%-response times of the sensor are about 32.1 min, 48.9 min, and 49.7 min, respectively. The specificity of the biosensor was tested by using Orf-1 DNA sequence as control DNA. As shown in Fig. 5e, the measured responses of the biosensor to the control DNA solutions at the concentrations of 100 ng/mL, 1 μg/mL, and 10 μg/mL are 0.247, 0.169, 0.05 times of the responses to target DNA, which indicate a good specificity of the sensor. To verify the sensor's effectiveness in the detection of target DNA in a solution with interfering DNA, the result of the detection of 10 pM target DNA mixed with 1 nM interfering DNA was measured and compared with the response to a control solution of 1 nM interfering DNA, as shown in Fig. S6. More results on the detection of Orf-1 DNA sequence are given in Fig. S7.

## 4. Discussion

SARS-CoV-2 antibody in serum is commonly tested by using the techniques with the LOD at the level of 0.04 ~ 0.30 μg/mL (Iyer, et al., 2020), which is comparable with this optical fiber-tip LSPR biosensor. Moreover, the LOD of the biosensor in the detection of SARS-CoV-2 mimetic DNA is ~0.8 pM, which is better than the reported fluorescence methods used in polymerase chain reaction (PCR) assay whose typical LOD is 9 ~ 20 pM (Xiang, et al., 2014; Peng, et al., 2017). Further consider that the actual size of SARS-CoV-2 RNA (with 29.9 kilobases) is about 302 times than the viral mimetic N-protein DNA sequence (with 99 bases) used in the experiment. According to the relationship between LSPR detection ability and target size (Qiu, et al., 2020), the LOD of the sensor for detection of SARS-CoV-2 RNA could be estimated to 2.7 fM, which is about $1.6\times10^6$ copies per mL. As the viral loads range from $1\times10^3$ to $1\times10^{11}$ RNA copies per swab or mL (Pujadas, et al., 2020; Pan, et al., 2020), this biosensor thus holds great promise for direct SARS-CoV-2 nucleic acid analysis.

The performance difference in the detection of antibody and DNA may mainly come from two causes. Firstly, the LSPR is a near-field interaction between incident light and electrons and decays exponentially with distance in the order of a few tens of nanometers (Coronado et al., 2011). The receptor molecules conjugated upon AuNPs in the detect antibody, including cysteamine (77.5 Da), glutaraldehyde (100.11 Da) and human IgG (150 kDa), is more than twenty times larger than that of the SH-DNA probe (7.1 kDa). It may produce a relatively far distance between LSPR and the interaction between human IgG and

goat anti-human IgG that leads to a lower sensitivity. Secondly, the equilibrium dissociation constant of immobilized antibodies to antigens is typically about $10^{-5} \sim 10^{-7}$ M (Tajima et al., 2011), which is much larger than that of DNA, about $10^{-9\sim} \times 10^{-11}$ M (Stevens et al., 1999). Moreover, the binding between glutaraldehyde and antigen protein human IgG formed during the functionalization of LSPR sensor for antibody detection is randomly oriented, in which the covalent immobilization process may reduce protein activity and thereby weakens the sensor's antibody detection sensitivity. On the contrary, in the functionalization of the LSPR sensor for DNA detection, SH-DNA probes are immobilized via one end of the single-stranded DNA by a sulfhydryl modification process and therefore a well-oriented SH-DNA probe layer is formed on the outer surface of AuNPs, which helps to improve biosensor's activity and sensitivity. Therefore, in case that it is highly demanded to reduce the difference in detection sensitivity between antibody and DNA, a one-step-oriented modification method can be applied in the preparation of biosensors for antibody detection (Huertas et al., 2020).

One of remarkable features of the optical fiber-tip plasmonic biosensor is its fast response. It might mainly result from two causes. Firstly, the biosensor is extremely small, i.e. a single-layer of AuNPs on the optical fiber core region with a diameter of 50 μm. If use antibody detection as an example, it is known that the diffusion coefficient of human IgG in 10-times-diluted serum is $4.4 \times 10^{-7}$ $cm^2$ $s^{-1}$ at 20 °C (Pokrić et al., 1979). Therefore, the diffusion length can be estimated as 94 ~ 281 μm after 10 ~ 30 min, which is significantly larger than either the axial thickness (i.e. 70 ~ 90 nm in thickness) or lateral dimension (i.e. 25 μm in radius) of the sensor. Secondly, the plasmonic nature of the sensor and the broadband visible light, which is from a halogen lamp (Color temp 3000 K, ASBN-W050F, Spectral Products, USA) covering the LSPR peak of AuNPs, i.e. 600 ~ 650 nm, used in the testing might cause photothermal effect. The power of light launched in to optical fiber is about 52 μw, and the light power density is 2.7 w/$cm^2$,

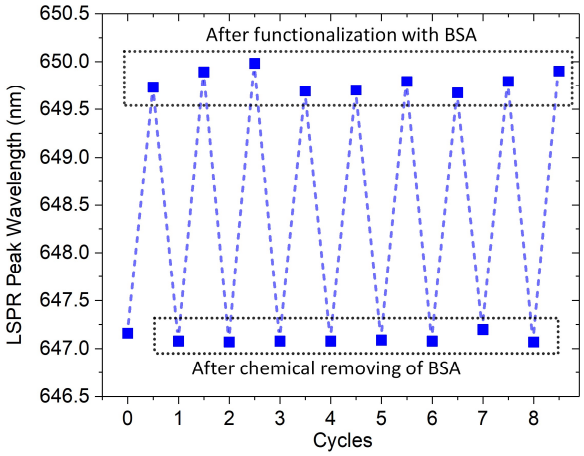


**Fig. 6.** Measured LSPR peak wavelengths of a fabricated optical fiber-tip plasmonic biosensor in 8 cycles of alternative functionalization with and chemical removal of BSA protein.

which is comparable with or higher than those with reported photothermal effect (Yue et al., 2016; Guo et al., 2017; Qiu et al., 2020). The increase of local temperature induced by photothermal effect may dramatically shorten a biosensor's response time (Qiu et al., 2020).

Notably, because of the high chemical stability of $TiO_2$ coating and AuNPs, the optical fiber-tip LSPR sensor can be chemically treated to remove the biomaterials immobilized on the surface of AuNPs for repeated use. Fig. 6 shows the experimental results on the reusability testing of a biosensor for 8 cycles. It can be seen that the LSPR peak wavelength can repeatedly shift forth and back according to the functionalization with BSA protein and chemical removal using 98% sulfuric acid, alternatively, which indicates that the optical fiber-tip LSPR sensor has great potential in the development of reusable biosensors. The shift of LSPR peak wavelength during the functionalization with BSA and the measured reflection spectra of the optical fiber-tip plasmonic sensor after chemically removing of BSA protein in 8 cycles of reusability testing are given in Fig. S8.

The optical fiber-tip plasmonic sensor is a universal label-free biosensing tool. In addition to antibody and DNA detection, it can be applied for the detection of many kinds of disease biomarkers as well as drugs, hormones and other biomolecular markers (Masson et al., 2017). The ultrasmall size, good performance and low cost make the sensor great potential in not only practical clinical diagnosis but also some emerging applications such as in vivo tissue biopsy and integrated wearable devices (Desroches et al., 2018, Altug et al., 2022).

## 5. Conclusions

We have presented an ultraminiature optical fiber-tip plasmonic biosensor based on plasmonic gold nanoparticles. An additive micro-printing technology based on an in-situ precision photoreduction technique has been developed to directly print size-controlled gold nanoparticles on the end face of optical fiber. It can not only enable the fabrication of such an ultraminiature optical biosensor, but also greatly reduce the fabrication cost by reducing the consumption of expensive precious metal materials. The optical fiber-tip plasmonic biosensor provides a universal plasmonic biosensing tool for many biodetection and diagnostic applications. Experiments have been demonstrated that the optical fiber-tip plasmonic sensor can be efficiently functionalized to detect goat anti-human IgG and N-protein DNA sequence at the LODs of 100 ng/mL and 0.8 pM, respectively, which indicates its great potential in SARS-COV-2 diagnostic and vaccine efficacy evaluation applications.

## Credit authorship contribution statement

Y.X.Z. and H. W. fabricated the sensors. Y.X. Z. conducted the numerical simulation. H.W. and B.H.Y. carried out the biodetection experiments. D. S.-H. W., A.P.Z and H.-Y.T. analyzed the data and provided feedback on the experiments. A.P.Z. conceived the experiments and wrote the manuscript. All authors were involved in writing the manuscript.

## Declaration of competing interest

The authors declare that they have no known competing financial interests or personal relationships that could have appeared to influence the work reported in this paper.

## Acknowledgments

The work was supported by the Local Innovative and Research Teams Project of Guangdong Pearl River Talents Program (Grant No.: 2019BT02X105) and a grant from the Research Grants Council of the Hong Kong SAR, China (Grant No.: PolyU 152215/18E).

## Appendix A. Supplementary data

Supplementary data to this article can be found online at XXX.XXX.

## References

Li, J., Liang, J.Y., Laken, S.J., Langer, R., Traverso, G., 2020. Clinical opportunities for continuous biosensing and closed-loop therapies. Trends Chem. 2(4), 319-340.

King, D.A., Peckham, C., Waage, J.K., Brownlie, J., Woolhouse, M.E., 2006. Epidemiology. Infectious diseases: preparing for the future. Science 313(5792), 1392-1393.

Wood, C.S., Thomas, M.R., Budd, J., Mashamba-Thompson, T.P., Herbst, K., Pillay, D., Peeling, R.W., Johnson, A.M., McKendry, R.A., Stevens, M.M., 2019. Taking connected mobile-health diagnostics of infectious diseases to the field. Nature 566(7745), 467-474.

Vandenberg, O., Martiny, D., Rochas, O., van Belkum, A., Kozlakidis, Z., 2021. Considerations for diagnostic COVID-19 tests. Nat. Rev. Microbiol. 19(3), 171-183.

Kevadiya, B.D., Machhi, J., Herskovitz, J., Oleynikov, M.D., Blomberg, W.R., Bajwa, N., Soni, D., Das, S., Hasan, M., Patel, M., 2021. Diagnostics for SARS-CoV-2 infections. Nat. Mater. 20(5), 593-605.

Surkova, E., Nikolayevskyy, V., Drobniewski, F., 2020. False-positive COVID-19 results: hidden problems and costs. Lancet Respir. Med. 8(12), 1167-1168.

Altug, H., Oh, S.-H., Maier, S.A., Homola, J., 2022. Advances and applications of nanophotonic biosensors. Nat. Nanotechnol. 17(1), 5-16.

Koenderink, A.F., Alu, A., Polman, A., 2015. Nanophotonics: Shrinking light-based technology. Science 348(6234), 516-521.

Mejía-Salazar, J., Oliveira Jr, O.N., 2018. Plasmonic biosensing: Focus review. Chem. Rev. 118(20), 10617-10625.

Zijlstra, P., Paulo, P.M., Orrit, M., 2012. Optical detection of single non-absorbing molecules using the surface plasmon resonance of a gold nanorod. Nat. Nanotechnol. 7(6), 379-382.

Brolo, A.G., 2012. Plasmonics for future biosensors. Nat. Photonics 6(11), 709-713.

Talebian, S., Wallace, G.G., Schroeder, A., Stellacci, F., Conde, J., 2020. Nanotechnology-based disinfectants and sensors for SARS-CoV-2. Nat. Nanotechnol. 15(8), 618-621.

Kostovski, G., Stoddart, P.R., Mitchell, A., 2014. The optical fiber tip: an inherently light-coupled microscopic platform for micro-and nanotechnologies. Adv. Mater. 26(23), 3798-3820.

Consales, M., Ricciardi, A., Crescitelli, A., Esposito, E., Cutolo, A., Cusano, A., 2012. Lab-on-fiber technology: toward multifunctional optical nanoprobes. ACS nano 6(4), 3163-3170.

Xiong, Y., Xu, F., 2020. Multifunctional integration on optical fiber tips: challenges and opportunities. Adv. photonics 2(6), 064001.

Tuniz, A., Schmidt, M.A., 2018. Interfacing optical fibers with plasmonic nanoconcentrators. Nanophotonics 7(7), 1279-1298.

Cennamo, N., Pasquardini, L., Arcadio, F., Lunelli, L., Vanzetti, L., Carafa, V., Altucci, L., Zeni, L., 2021. SARS-CoV-2 spike protein detection through a plasmonic D-shaped plastic optical fiber aptasensor. Talanta 233, 122532.

Caucheteur, C., Guo, T., Liu, F., Guan, B.-O., Albert, J., 2016. Ultrasensitive plasmonic sensing in air using optical fibre spectral combs. Nat. Commun. 7(1), 1-8.

Ermatov, T., Noskov, R.E., Machnev, A.A., Gnusov, I., Atkin, V., Lazareva, E.N., German, S.V., Kosolobov, S.S., Zatsepin, T.S., Sergeeva, O.V., 2020. Multispectral sensing of biological liquids with hollow-core microstructured optical fibres. Light Sci. Appl. 9(1), 1-12.

Bandaru, R., Divagar, M., Khanna, S., Danny, C.G., Gupta, S., Janakiraman, V., Sai, V., 2020. U-bent fiber optic plasmonic biosensor platform for ultrasensitive analyte detection. Sens. Actuators B Chem. 321, 128463.

Guggenheim, J.A., Li, J., Allen, T.J., Colchester, R.J., Noimark, S., Ogunlade, O., Parkin, I.P., Papakonstantinou, I., Desjardins, A.E., Zhang, E.Z., 2017. Ultrasensitive plano-concave optical microresonators for ultrasound sensing. Nat. Photonics 11(11), 714-719.

Kim, J.A., Wales, D.J., Thompson, A.J., Yang, G.Z., 2020. Fiber-optic SERS probes fabricated using two-photon polymerization for rapid detection of bacteria. Adv. Opt. Mater. 8(9), 1901934.

Kostovski, G., Chinnasamy, U., Jayawardhana, S., Stoddart, P.R., Mitchell, A., 2011. Sub-15nm Optical Fiber Nanoimprint Lithography: A Parallel, Self-aligned and Portable Approach. Adv. Mater. 23(4), 531-535.

Sanders, M., Lin, Y., Wei, J., Bono, T., Lindquist, R.G., 2014. An enhanced LSPR fiber-optic nanoprobe for ultrasensitive detection of protein biomarkers. Biosens. Bioelectron. 61, 95-101.

Principe, M., Consales, M., Micco, A., Crescitelli, A., Castaldi, G., Esposito, E., La Ferrara, V., Cutolo, A., Galdi, V., Cusano, A., 2017. Optical fiber meta-tips. Light Sci. Appl. 6(3), e16226-e16226.

Zhang, Y., Zhang, Q., Ouyang, X., Lei, D.Y., Zhang, A.P., Tam, H.-Y., 2018. Ultrafast light-controlled growth of silver nanoparticles for direct plasmonic color printing. ACS nano 12(10), 9913-9921.

Zhang, Y., Liang, Z., Zhang, A.P., Tam, H.Y., 2021. Direct Printing of Micropatterned Plasmonic Substrates of Size-Controlled Gold Nanoparticles by Precision Photoreduction. Adv. Opt. Mater. 9(1), 2001368.

Mie, G., 1908. Beiträge zur Optik trüber Medien, speziell kolloidaler Metallösungen. Ann. Phys. 330(3), 377-445.

Gans, R., 1912. Über die form ultramikroskopischer goldteilchen. Ann. Phys. 342(5), 881-900.

Bobbert, P., Vlieger, J., 1986. Light scattering by a sphere on a substrate. Phys. A: Stat. Mech. Appl. 137(1-2), 209-242.

Ungureanu, C., Rayavarapu, R.G., Manohar, S., van Leeuwen, T.G., 2009. Discrete dipole approximation simulations of gold nanorod optical properties: Choice of input parameters and comparison with experiment. J. Appl. Phys. 105(10), 102032.

Maier, S.A., 2007. Plasmonics: fundamentals and applications. Springer.

Zhu, X.-P., Zhang, S., Shi, H.-M., Chen, Z.-Q., Quan, J., Xue, S.-W., Zhang, J., Duan, H.-G., 2019. Research progress of coupling theory of metal surface plasmon. Acta Phys. Sin. 68(24), 247301.

Chauhan, M., Singh, V.K., 2021. Review on recent experimental SPR/LSPR based fiber optic analyte sensors. Opt. Fiber Technol. 64, 102580.

Tumolo, T., Angnes, L., Baptista, M.S., 2004. Determination of the refractive index increment (dn/dc) of molecule and macromolecule solutions by surface plasmon resonance. Analytical biochemistry 333(2), 273-279.

Iyer, A.S., Jones, F.K., Nodoushani, A., Kelly, M., Becker, M., Slater, D., Mills, R., Teng, E., Kamruzzaman, M., Garcia-Beltran, W.F., 2020. Persistence and decay of human antibody responses to the receptor binding domain of SARS-CoV-2 spike protein in COVID-19 patients. Sci. Immunol. 5(52), eabe0367.

Sheikhzadeh, E., Eissa, S., Ismail, A., Zourob, M., 2020. Diagnostic techniques for COVID-19 and new developments. Talanta 220, 121392.

Xiang, D., Zhai, K., Xiang, W., Wang, L., 2014. Highly sensitive fluorescence quantitative detection of specific DNA sequences with molecular beacons and nucleic acid dye SYBR Green I. Talanta 129, 249-253.

Peng, Y., Huang, Y., Zhu, Y., Chen, B., Wang, L., Lai, Z., Zhang, Z., Zhao, M., Tan, C., Yang, N., 2017. Ultrathin two-dimensional covalent organic framework nanosheets: preparation and application in highly sensitive and selective DNA detection. J. Am. Chem. Soc. 139(25), 8698-8704.

Qiu, G.G., Gai, Z.B., Tao, Y.L., Schmitt, J., Kullak-Ublick, G.A., Wang, J., 2020. Dual-Functional Plasmonic Photothermal Biosensors for Highly Accurate Severe Acute Respiratory Syndrome Coronavirus 2 Detection. ACS nano 14(5), 5268-5277.

Pujadas, E., Chaudhry, F., McBride, R., Richter, F., Zhao, S., Wajnberg, A., Nadkarni, G., Glicksberg, B.S., Houldsworth, J., Cordon-Cardo, C., 2020. SARS-CoV-2 viral load predicts COVID-19 mortality. Lancet Respir. Med. 8(9), E70-E70.

Pan, Y., Zhang, D.T., Yang, P., Poon, L.L.M., Wang, Q.Y., 2020. Viral load of SARS-CoV-2 in clinical samples. Lancet Infect. Dis. 20(4), 411-412.

Coronado, E.A., Encina, E.R., Stefani, F.D., 2011. Optical properties of metallic nanoparticles: manipulating light, heat and forces at the nanoscale. Nanoscale 3(10), 4042-4059.

Tajima, N., Takai, M., Ishihara, K., 2011. Significance of antibody orientation unraveled: well-oriented antibodies recorded high binding affinity. Anal. Chem. 83(6), 1969-1976.

Stevens, P.W., Henry, M.R., Kelso, D.M., 1999. DNA hybridization on microparticles: determining capture-probe density and equilibrium dissociation constants. Nucleic Acids Res. 27(7), 1719-1727.

Huertas, C.S., Soler, M., Estevez, M.-C., Lechuga, L.M., 2020. One-step immobilization of antibodies and DNA on gold sensor surfaces via a poly-adenine oligonucleotide approach. Anal. Chem. 92(18), 12596-12604.

Pokrić, B., Pučar, Z., 1979. The two-cross immunodiffusion technique: diffusion coefficients and precipitating titers of IgG in human serum and rabbit serum antibodies. Anal. Biochem. 93, 103-114.

Yue, K., Nan, J., Zhang, X., Tang, J., Zhang, X., 2016. Photothermal effects of gold nanoparticles induced by light emitting diodes. Appl. Therm. Eng. 99, 1093-1100.

Guo, A., Fu, Y., Wang, G., Wang, X., 2017. Diameter effect of gold nanoparticles on photothermal conversion for solar steam generation. RSC Adv. 7(8), 4815-4824.

Masson, J.-F., 2017. Surface plasmon resonance clinical biosensors for medical diagnostics. ACS Sens. 2(1), 16-30.

Desroches, J., Jermyn, M., Pinto, M., Picot, F., Tremblay, M.-A., Obaid, S., Marple, E., Urmey, K., Trudel, D., Soulez, G., Guiot, M.-C., Wilson, B. C., Petrecca, K., Leblond, F., 2018. A new method using Raman spectroscopy for in vivo targeted brain cancer tissue biopsy. Sci. Rep. 8, 1-10.

Altug, H., Oh, S.-H., Maier, S.A., Homola, J., 2022. Advances and applications of nanophotonic biosensors. Nat. Nanotechnol. 17(1), 5-16.